Evidence for Secondary Minimum Flocculation of Stöber Silica Nanoparticles at the Air−Water Interface: Film Balance Investigations and Computer Simulations

G. Tolnai,[†,‡] A. Agod,[†] M. Kabai-Faix,[†] A. L. Kovács,[§] J. J. Ramsden,[||] and Z. Hórvölgyi*[,†]

Department of Physical Chemistry, Budapest University of Technology and Economics, H-1521, Budapest, Hungary, Cell Physiology Laboratory POB 120, Department of General Zoology, Loránd Eötvös University, H-1518 Budapest, Hungary, and Department of Advanced Materials, Cranfield University, MK43 0AL, England

Received: February 26, 2003; In Final Form: July 3, 2003

The interactions of Stöber silica nanospheres having diameters of ca. 40, 100, and 200 nm were studied at the water−air interface with a Wilhelmy film balance. The particle sizes and size distribution functions were determined from TEM measurements. According to in situ Brewster angle microscopy investigations and the calculated DLVO interparticle energies, the particles formed weakly cohesive films at the interface; hence, the increasing surface pressure during the compression was attributed to interparticle repulsion. The repulsion energies that were determined from the surface pressure versus surface area isotherms exceeded the calculated DLVO energies by 2−3 orders of magnitude. The extremely high interparticle repulsion was attributed to dipole−dipole interactions. Despite the high interparticle repulsion, the monolayer of the particles was in a weakly cohesive state prior to compression that was attributed to the recently recognized long-range attractions of capillary and electrostatic origin. The particle size dependent particle−particle (p−p) distances at the secondary energy minimum of total pair-interaction versus p−p distances curve were also interpreted in terms of the newly recognized interactions. A computer simulation-assisted method was proposed to estimate the error of assuming a hexagonal array of monodisperse particles, which was then taken into account in the calculation of the p−p distances determined from the pressure−area isotherms.

Introduction

The interactions of colloid particles in two dimensions have been the subject of extensive theoretical and experimental investigations for many decades. Because of numerous practical and theoretical reasons,[1] the stability of interfacial colloids also attracted significant attention.

The "two-dimensional" systems served as models for the investigation of general aspects of growth,[2−17] structure formation,[18−24] phase transitions,[25] and surface thermodynamics.[25−29] In other cases, the investigations focused on the practical applications such as thin-layer preparation[30−35,20] and particle characterization.[36−38] The interfacial colloids may also have significant importance in well-known technologies such as froth flotation.[39−40]

The measurement of the effective surface tension of a monoparticulate layer using a film balance or by another way can provide an experimental tool for the study of particle−particle (p−p) interactions at liquid−fluid interfaces.[41−46] Though the method has been known for about forty years, it could not spread widely because of many difficulties (contaminations of model particles,[42−43] particle loss due to the spreading process, cohesive film formation due to the hydrophobic forces,[47−49] etc.) and the lack of suitable model particles. In certain cases, the synthesized polymeric particles have hairy surfaces[50] that cause further difficulties in the interpretation of the experimental results.

Despite the above difficulties, successful film balance experiments were reported concerning the determination of interparticle repulsion energies by using polymeric (140−610 nm diameter)[43,44] and 2−8 nm diameter $CaCO_3$ particles.[45] Every calculation was carried out considering the array of monodisperse particles during compression to be hexagonal.

Recently, the structure formation, the collapse mechanism, and the interparticle forces of monodisperse polystyrene spheres (with diameter of 0.21−2.6 μm) were studied at water−air and water−octane interfaces on a Langmuir trough.[51−52] The investigations revealed a buckling type collapse mechanism without particle loss from the boundary layer and showed a very long-range interparticle repulsion at the water−octane interface. The repulsion was attributed to the Coloumbic interaction between residual charges at the particle−oil interface. Such a great repulsion was not reported between latex particles at the water−air interface presumably because of the relatively low value of the particle−water contact angles (below 30°).[51]

Nowadays, computer simulation of monoparticulate films compressed on a Langmuir trough also became a powerful tool to study the particle−particle interactions[53,54] and in comparison with experimental results,[52] it provided useful information about the theoretically introduced and long-range dipole−dipole and residual surface charge repulsions[55−56,13] between the interfacial particles.

The synthesis of silica particles by controlled hydrolysis of tetraethyl-orthosilicate (TEOS) in ethanol (in the presence of aqueous ammonia) has been known for more than thirty years.[57] The so-called Stöber silica has many advantageous properties

* Corresponding author. E-mail: horvolgyi.fkt@chem.bme.hu; tel.: 36 1 463 2911; fax: 36 1 463 3767.

[†] Budapest University of Technology and Economics.

[‡] Present address: Department of Nanostructures and Surface Modification, CRC HAS, H-1525 Budapest, P. O. B. 17.

[§] Loránd Eötvös University.

[||] Cranfield University.

10.1021/jp0344949 CCC: $25.00
Published on Web 09/16/2003

TABLE 1: Preparation of Model Particles

samples	TEOS (cm^3)	aqueous NH_3−solution (cm^3)	ethanol (cm^3)
S40	10	10	250
S100	10	15	250
S200	10	20	250

for model investigations. The near spherical, inorganic particles show narrow size distribution and are compact above a certain particle size (ca. 20 nm diameter).[58] Moreover, the particles can be transferred into water from the alcoholic phase and the hydrosol was stable without any additives[59] because of a stabilizing water film between the surface of the particles. On the other hand, the mixture of alcosol and chloroform can be spread at water−air interface and the particles form a monoparticulate layer without significant loss of particles, as was shown earlier.[20,24] The partial wetting of native Stöber silica particles can be attributed to the presence of non-hydrolyzed ethoxy-groups and the "Si−O−Si" parts of the silica surface.

Though weakly cohesive films of interfacial colloids frequently occur in practice, their behavior has been scarcely studied in model investigations. The purpose of this work is to study the interparticle energies of Stöber silica particles that formed a weakly cohesive layer at the water−air interface without any stabilizing agents. We measured the pressure−area isotherms by using a Wilhelmy film balance and calculated the DLVO energies to get information about the role of the non-DLVO forces in the stabilization. For comparison, we investigated the repulsion energies at three different particle sizes, ca. 40, 100, and 200 nm diameters, and at different amounts of spread particles. The long-range structure and dispersibility of the particulate layer was studied by Brewster-angle microscopy. The p−p distances at the secondary minima of the total interparticle energies were approximated from the pressure−area isotherms and corrected by computer simulations assessing the error originating in the usage of the hexagonal array of monodisperse particle model in the calculation.

In the next part of the paper, we survey the materials and the experimental and simulation methods and then give a short summary of the model calculations.

Materials and Methods

Materials. For the synthesis of Stöber silica tetraethyl orthosilicate (TEOS, >98% GC, Fluka), absolute ethanol (A. R., >99.7%, Reanal) and ammonium hydroxide (25% aqueous solution of NH_3, A. R., Reanal) were used as received. For the film balance experiments, chloroform (>99.8%, "Baker Resy Analyzed", J. T. Baker Inc.) and distilled water (Millipore Milli Q) were used.

Instruments and Experimental Methods. *Preparation of Stöber Silica Particles.* The alcosol of silica particles was prepared according to the Stöber method.[57] By choosing appropriate reagent concentrations, (Table 1), spheres of diameter ca. 200 nm (batch S200), ca. 100 nm (batch S100), and ca. 40 nm (batch S40) were prepared. The solid content of the alcosols (mg/ml) was determined from the amount of residual solid after solvent evaporation in a drying oven at 80 °C.

Particle Size Measurements. A JEOL JEM-100 CX II transmission electron microscope was used to assess the particle size and shape. The samples were deposited on Formvar film-coated carrier grids. Particle sizes were determined by measuring the diameters (d_i) of 400−500 spherical particles from which the particle size distribution was determined.

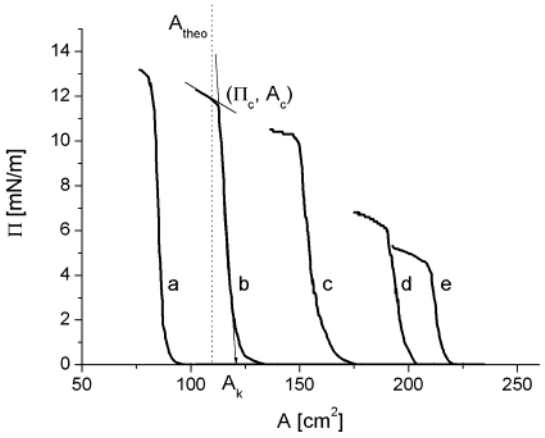

Figure 1. Particle size distribution function for S200 sample (determined from TEM measurements).

On the basis of the distribution, the sphere-equivalent parameters of mean diameter ($\bar{q}$), mean cross section ($\bar{A}$), and mean volume ($\bar{V}$) of the particles were calculated as follows:

$$\bar{q} = \frac{1}{N}\sum_{i=1}^{N} d_i \tag{1}$$

$$\bar{A} = \frac{\pi}{4N}\sum_{i=1}^{N} d_i^2 \tag{2}$$

$$\bar{V} = \frac{\pi}{6N}\sum_{i=1}^{N} d_i^3 \tag{3}$$

where N is the number of particles used for the calculations. The number of spread particles (Z) was determined from the spread amount (m_{tot}) of particles by the following equation:

$$Z = m_{tot}/(\rho\bar{V}) \tag{4}$$

where $\rho = 2060$ kg/m^3.[59]

Film Balance Experiments. A laboratory-built Wilhelmy film balance was used to determine the surface pressure (Π) versus surface area (A) isotherms of monoparticulate layers at ambient temperature (23 ± 1 °C). The sols for spreading were prepared by diluting the silica suspensions with chloroform (1 vol alcosol + 2 vol chloroform) and then homogenizing in an ultrasonic bath for 10 min. An appropriate amount of sol was spread on the surface of water in the film balance. After the evaporation of the spreading liquid, the $\Pi-A$ isotherms were obtained at a rate of 3.35 cm/min of the moving barrier (corresponding to 33.5 cm^2/min). To assess the reproducibility, the film balance experiments were repeated five times in most cases by spreading the same volume of the sol.

Previously, it was found that the collapse pressure and contact angles of hydrophobic particles significantly depend on the amount of spread particles.[48] The effect was attributed to a surface pressure gradient along the very cohesive particulate layer. A more moderate mass dependence, as expected, was found for the less hydrophobic silica particles.[48] To take this effect into consideration, we measured the $\Pi-A$ isotherms by spreading different amounts of particles for every sample. The water contact angles for the characterization of the particles' surfaces were determined from the $\Pi-A$ isotherms[60] using the collapse pressure (Π_c) and collapse area (A_c) data (Figure 1) by an extrapolation method.[48]

Brewster Angle Microscopy (BAM). A laboratory-built Brewster angle microscope[61,20] was used to obtain in situ information about the long-range structure of the silica particulate layer formed at the water surface in the film balance. Illumination was provided by a plane-polarized He−Ne laser (Melles Griot, $\lambda = 632.8$ nm, 17 mW) which was used in p-polarized mode at the Brewster angle of incidence (≈53° for water−air). The beam reflected from the nanolayer was detected by a monochrome CCD video camera, which was coupled to a computer via an Adobe digitizing card for image processing. The video microscope was supplied with an objective lens having magnification of 2.5. To get an insight into the dispersibility of particles, the images were taken at zero surface pressure and during the compression and expansion cycle, as well.

Model Calculation of Interparticle Energies. The total pair-interaction energy for interfacial particles floating at liquid−gas interfaces can be written in the following form:

$$V_T = V_A + V_R + V_S + V_D \tag{5}$$

where V_A is the van der Waals attraction, V_R is the electric-double-layer repulsion, and V_S is the structural[47] (or acid−base[62]) interaction energy. This last one can be either attractive (hydrophobic attraction energy) or repulsive (solvation repulsion energy) depending on the hydrophobic−hydrophilic nature of the particles' surface. If the water contact angle is lower than 15°, the surface will be hydrophilic and above 64° it should be considered as hydrophobic.[63] It means that the DLVO theory gives reasonable results for surfaces with water contact angles between ca. 15 and 65°. V_D is the dipole−dipole (and monopole−monopole or monopole−dipole) repulsion energy[64,55,13] which was introduced theoretically as a consequence of the asymmetrical electric double layer around the floating particles at water−fluid interface whose significance has been intensively studied recently.[53,63−64] The "floating type" of capillary attraction energies at the present sizes of particles can be neglected.[65]

Determination of the Total Interparticle Repulsive Energies (V_T) by the Analysis of $\Pi-A$ Isotherms. The total (repulsive) pair-potential energies were calculated by integrating the $\Pi-A$ isotherms supposing a hexagonal array of monodisperse spheres during compression and expecting that only the nearest neighbor interactions are significant:

$$V_T = -\frac{1}{3}\int_{A_\infty}^{A_H} \Pi(A')dA' \tag{6}$$

where A' is the area for a particle and A_H is the area for a particle in the monoparticulate layer at an interparticle distance of H. H relates to A_H as follows:

$$H = 2\left(\sqrt{\frac{A_H}{6\tan\left(\frac{\pi}{6}\right)}} - a\right) \tag{7}$$

where a is the radius of the spherical particles. For the calculation of A_H, the amount and density (2060 kgm^{-3})[59] of spread particles is required. We get the total pair-interaction energy as a function of H by comparing eq 6 with eq 7.

Calculation of DLVO Energies ($V_A + V_R$). V_A was approximated by the following expression:

$$V_A = -Ca/12H \tag{8}$$

where C is the compound Hamaker constant for silica-in-water obtained from the literature (4×10^{-21} J).[66] If the thickness of the electric double layer is commensurate with the particle size, V_R can be approximated as:[67]

$$V_R = \epsilon a \Psi_0^2 \exp[-\tau(s-2)]/s \tag{9}$$

where ϵ is the absolute permittivity of water (7.1×10^{-10} C/Vm); Ψ_0 is the surface potential that was replaced with the experimentally determined value of zeta potential (−40 mV);[68] $\tau = \kappa$a, where κ is the reciprocal Debye−Hückel parameter to be taken as $10^7 - 10^8$ m^{-1}; $s = (H + 2a)/a$. Equation 9 does not take into consideration the differences between the constant surface potential and constant surface charge density conditions.[67] Applying eq 8 and 9 we consider that the particles are totally immersed in the aqueous phase. This consideration will be verified in a later part of the text.

Computer Simulation. We have run molecular dynamics-based computer simulations to improve our understanding of the pressure−surface area isotherms. The motion of the particles was derived from Newton's equations by the leapfrog integration method.[69] To study the compression of the particles, we have used 1000 particles of the experimentally determined size distribution in a rectangular area and have considered a periodic boundary condition. The particle−particle interactions have been derived from the isotherms of the real experiments by the method described in the previous section. We have considered the potential of the interaction to be determined by the distance between two particles' surfaces and independent of the particle size. We have cut off the potential ($V = 0$) if the experimentally derived potential values were less than 0.1 kT.

The compression of the layer has been simulated by successively reducing the area of the simulation cell by 0.5% and rescaling the positions of the particles. For the numerical integration of the equations of the motion, we have used 10^{-11} s time steps. For each compression step, the system reached a (quasi) equilibrium state in approximately $M = 800$ time steps. To keep the system at a fixed (room) temperature, we also had to rescale the velocity of the particles since $1/2\sum_{i=1}^{N} m_i v_i^2 = NkT$ (m_i is the mass of the ith particle). We have used the virial theorem to calculate the surface pressure of the layer.[69]

$$\Pi = n\frac{\left\langle \sum_{i=1}^{N} m_i v_i^2 + \sum_{(i,j)} \vec{F}_{ij}\vec{r}_{ij} \right\rangle}{2N} = \frac{NkT}{A} + \frac{1}{2A}\left\langle \sum_{(i,j)} \vec{F}_{ij}\vec{r}_{ij} \right\rangle \tag{10}$$

where $\vec{r}_{ij} \cong \vec{r}_i - \vec{r}_j$ is the separation between the mass centers of particles i and j, (i,j) are the interacting pairs, $\vec{F}_{ij}$ is the force between particles i and j (derived from the interaction potential), $n = N/A$, v_i is the velocity of particle i, k is the Boltzmann constant, T is the ambient temperature.

Results and Discussion

In this section, we will survey our results concerning the particle properties (size and wettability), the stability of the 2D sol, the calculated and experimentally determined interparticle energies, and finally the computer simulations.

Particle Sizes from the TEM Examinations. For demonstration, the TEM images of synthesized particles and the particle size distribution function of the S200 sample is depicted in Figure 2a−c and in Figure 3, respectively. The experimentally determined particle sizes appear in Table 2. It can be seen that the real particle sizes correlate well to the planned values.

The Analysis of $\Pi-A$ Isotherms: Particle Wettability. The surface pressure below the collapse pressure showed a slight

Figure 2. TEM images (from top to bottom) taken about the S40, S100, and S200 particles. The magnification is 80000× (S40), 50000× (S100), and 27000× (S200).

decrease keeping constant the surface area (ca. 0.1 mN/m·min). Similar behavior was found earlier for weakly cohesive layers of microparticles.[38] The $\Pi-A$ isotherms were not reproducible if the samples were compressed beyond the collapse pressure showing the irreversible removal of particles from the interface. During the collapse, however, whitish folds were not observed, which means the particles sank into the aqueous phase irreversibly. Hence, we could determine the advancing water contact angles from the $\Pi-A$ isotherms. In Figure 1, characteristic $\Pi-A$ isotherms are shown for the smallest particles (sample S40). The collapse pressure can be seen to increase with decreasing amount of particles. We give the values of collapse pressure and contact angles for the investigated samples in Table 2. The values of collapse pressures are relatively low, not exceeding 15 mN/m, as expected for weakly cohesive layers,[48] but show a significant increase with a decreasing amount of particles in every case.

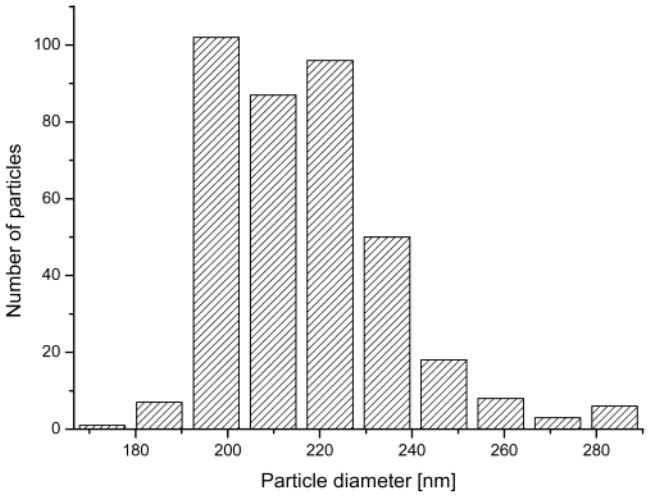

Figure 3. Surface pressure (Π) vs surface area (A) isotherms of S40 sample obtained at different amounts of spread particles. Π_c: collapse pressure; A_c: collapse area; A_k: contact cross-sectional area; A_{theo}: the area covered by monodispersed spheres in most close-packed hexagonal array. The amounts of spread particles: 0.4 mg (a), 0.6 mg (b), 0.7 mg (c), 0.9 mg (d), 1.1 mg (e).

TABLE 2: Particle Properties (Particle Size and Water Wettability)[a]

	mean particle diameter (nm)	collapse pressure (mN/m)	Θ_m[b]	Θ_{ext} ($m \rightarrow 0$, $\Theta_m \rightarrow \Theta_{ext}$)
m_{S40} (mg)				
0.4	44 ± 8	13.6	60°	69°
0.6		11.3	56°	
0.7		10.7	56°	
0.9		6.2	48°	
1.1		4.5	43°	
m_{S100} (mg)				
0.8	97 ± 17	13.4	59°	65°
1.3		10.3	55°	
1.8		8.8	52°	
2.3		5.0	44°	
m_{S200} (mg)				
2.8	214 ± 18	11.3	55°	61°
3.2		10.3	54°	
3.5		9.5	53°	
3.8		8.8	52°	
4.4		8.7	51°	
4.8		8.6	51°	

[a] The mean particle diameters of different samples and collapse pressures, advancing water contact angles (Θ_m) at different amounts (m) of spread particles. Θ_{ext}: the extrapolated and characteristic contact angle. [b] The standard deviation of contact angles was ±1°.

From the advancing contact angles in Table 2 (61° − 69°), hydration repulsion cannot be predicted (cf. with the previous section, Model Calculation of Interparticle Energies). The bigger particles show more hydrophilic character. This may relate to the water and ammonia content of the reaction medium (Table 1). The bigger particles are prepared in a more aqueous and basic environment that can facilitate the hydrolysis of ethoxy groups resulting in forming more silanol groups at the surface.

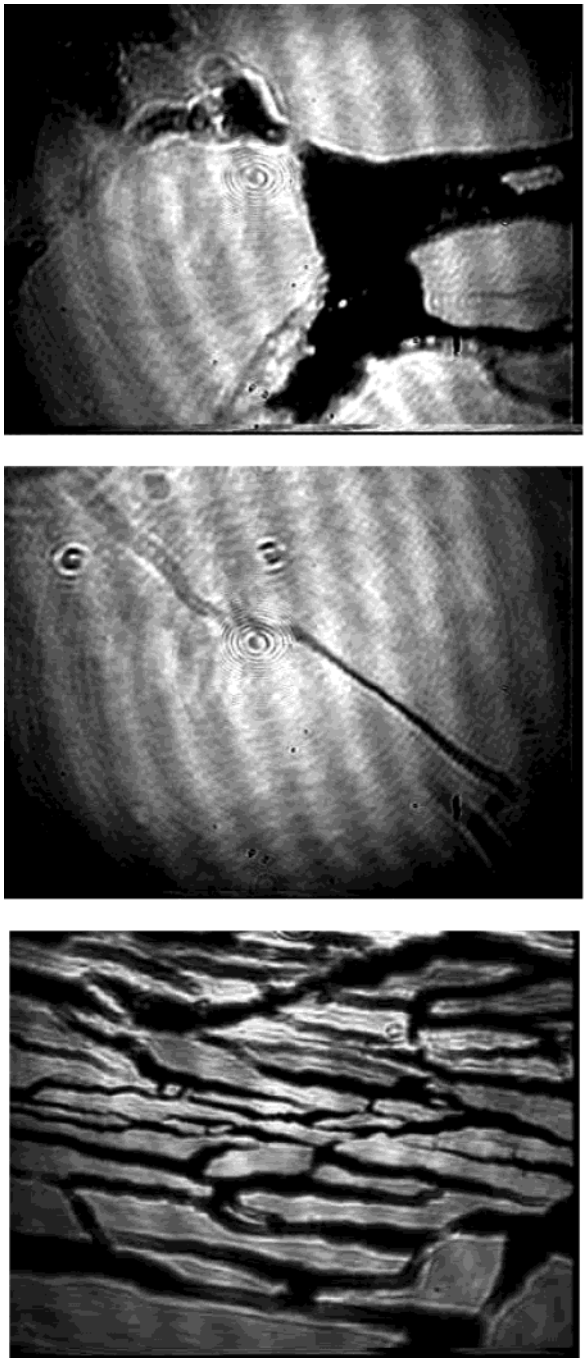

Figure 4. Brewster angle microscope images of S40 sample (from top to bottom) taken at the zero surface pressure after spreading, at around the collapse and during the decompression. The width of the pictures corresponds to ca. 550 μm.

The wettability also has relevance in the calculation of DLVO energies. For nanosized particles, neglecting the effect of gravitation, the immersion depth of particles q (given in units of particle radius) can be calculated by the following expression:[70]

$$q = 1 + \cos \Theta_A \qquad (11)$$

where Θ_A is the advancing contact angle. For the present particles, the immersion depth is around 1.4−1.5 particle radius. In this case, the pair-potential (eq 9) for the calculation of the electric-double-layer repulsion energy can be used without any modification as if the spheres totally were in the aqueous phase.[71] This approximation is also acceptable for the calculation of the attractive dispersion energy.[63]

TABLE 3: Characteristic Parameters of Interparticle Interactions[a]

samples	V_T(max)[b] (kT)	H_c (nm)	$(F/r)_c$ (mN/m)	H_{l0} and (H_{l0corr}) (nm)
S40	1.5 (H = 2.5 nm)	2.6 ± 1.1	22	6.6 (4.4)
S100	5.5 (H = 3.6 nm)	3.4 ± 0.6	22	13.0 (9.4)
S200	11.4 (H = 5.2 nm)	8.4 ± 2.2	18	16.4 (13.6)

[a] V_T(max): the maximum value of calculated DLVO energies; H_c: p−p distances (extrapolated) at the collapse; $(F/r)_c$: the maximum (extrapolated) values of normalized repulsive interparticle forces at the collapse pressure; H_{l0}: extrapolated values of p−p distances at the secondary energy minimum of pair-interaction vs p−p distance function; H_{l0corr}: corrected H_{l0} values (assessed by computer simulation). [b] The DLVO energies were calculated by taking the values of 10^8 m^{-1} and 4×10^{-21} J for κ and C, respectively. Significant differences in DLVO energies were not found by using different values of κ and C. V_T (max), e.g., was 2.2 kT at $\kappa = 10^7$ m^{-1} keeping the value of C constant for sample S40 particles.

The Weakly Cohesive Nature of the Particulate Layer: BAM Investigations and DLVO Interparticle Energies. *BAM Investigations.* In Figure 4a−c, some characteristic BAM images of the layers of 44 nm particles are shown. As can be seen in Figure 4a, particulate domains (white) and clean water surface (dark) appear to show the flocculated state of particles before compression. The particulate layer becomes contiguous following the compression (Figure 4b). The homogeneous film can, however, be spontaneously dispersed into smaller parts (Figure 4c) by withdrawing the moving barrier. This implies a weakly cohesive layer. Other experimental results also support this idea. It was found previously[20] that similarly hydrophilic (advancing water contact angles of 70°) Stöber silica nanoparticles can easily be ordered into hexagonally packed arrays by compressing the particles in a Langmuir trough. Relating to this observation, the $\Pi-A$ isotherms are significantly steeper at this particle wettability than that of the hydrophobic particles,[20,38] also indicating that the less hydrophobic particles cannot form cohesive layer at the water−air interface. Although they are in flocculated state, as can be seen in the BAM image (Figure 4a), there can be a thin liquid film between them, that is, the particles can be in a secondary energy minimum.

The Calculated DLVO Energies. The calculated DLVO energies at different p−p distances reveal a maximum in the total pair-interaction energy versus p−p distance function. The maximum values of calculated DLVO energies and the corresponding p−p distances (in the brackets) are collected in Table 3. As can be seen, both the energies and distances increase with increasing particle sizes in the range of 1.5−11.4 kT and 2.5−5.2 nm. The energies in the secondary energy minimum were always smaller than 0.1 kT for all particle sizes.

The flocculated state of particles in a secondary energy minimum can be the consequence of the recently recognized long-range attractions of the floating particles. These attractions can be attributed to a capillary force due to the irregular shape of the three-phase contact line around the spheres[72] or to electrostatic forces[19] due to the periodic arrangement of counterions and charged particles.

The Analysis of $\Pi-A$ Isotherms: Interparticle Interactions. *The Assessment of the Non-DLVO Interactions.* As was mentioned above, the pressure−area isotherms significantly depend on the amount of spread particles. Because of this, the repulsion energies, calculated from the isotherms at numerous p−p distances, were extrapolated to zero amount of particles that resulted in an extrapolated energy versus p−p distance function. The resulting function for the 40 nm particles is depicted in Figure 5. (A similar function was obtained for

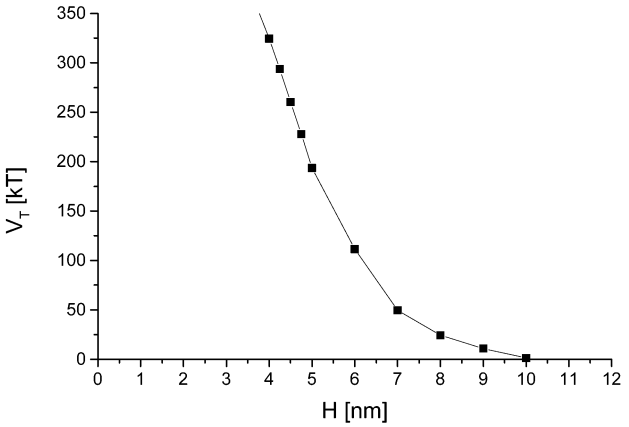

Figure 5. The experimentally determined (and extrapolated) total pair-interaction energy (V_T) vs particle−particle distance (H) function for sample S40.

sample S100 but we could not determine such a function for sample S200 because of the insufficient number of measurements data.)

We can come to the conclusion, comparing the energy values in Figure 5 with the maximum values of DLVO energies in Table 3, that the experimentally obtained repulsion energies are greater than the calculated ones by 2−3 orders of magnitude. Similar conclusion can be drawn for the bigger particles. For sample S200, the analysis of pair-potential energy functions at certain amounts of spread particles also led to this conclusion.

We also calculated the extrapolated values of p−p distances (H_c, Table 3) and of the repulsive interparticle forces according to ref 45 at the collapse from the pressure−area isotherms for comparison with data from the literature. The resultant force values normalized by the particle radius, $(F/r)_c$, can also be seen in Table 3. Such great repulsive forces (18−22 mN/m) at these p−p distances (ca. 2.6−8.4 nm) have not yet been observed from surface force apparatus (SFA) measurements even of hydrophilic surfaces,[73] a finding that also reveals the specific properties of interfacial colloids.

The Determination of the p−p Distances (H_l) at the Secondary Minimum of Interparticle Energies. In Figure 1, the important parameters, A_k and A_{theo}, can also be seen. For weakly cohesive particulate films, A_k (the contact cross-sectional area[38,74]) can be related to the p−p distance at the secondary minimum of interparticle energies (H_l). It can be determined by extrapolating the first, nearly linear part of the $\Pi-A$ isotherms to zero surface pressure (see Figure 1). The other important parameter is A_{theo}, the area covered by the monodisperse spheres in a hexagonal, most close-packed array, which corresponds to $\{\pi/(2\sqrt{3})\}$ (i.e., 90.7%) surface coverage of particles. A_{theo} in Figure 1 belongs to the second isotherm from the left-hand side. If the film shows hexagonal ordering and A_k is greater than A_{theo}, then significant repulsion exists among the particles compressing them to smaller areas than A_k. In the present cases, A_k was always greater than A_{theo}; hence, the interparticle repulsion energies versus p−p distances could be calculated by using eq 6 and eq 7.

The p−p distances at the secondary minimum of the interparticle energies (H_l) were approximated by dividing A_k the number of particles (Z), from which the H_l values were determined by using eq 7. We also determined H_l for all the systems as a function of spread amounts of particles. The results at different particle sizes can be seen in Figure 6a−c with symbol (■). The observed dependence of H_l on the amount of spread particles can be attributed to the above-mentioned surface pressure gradient along the layer that manifests itself in a

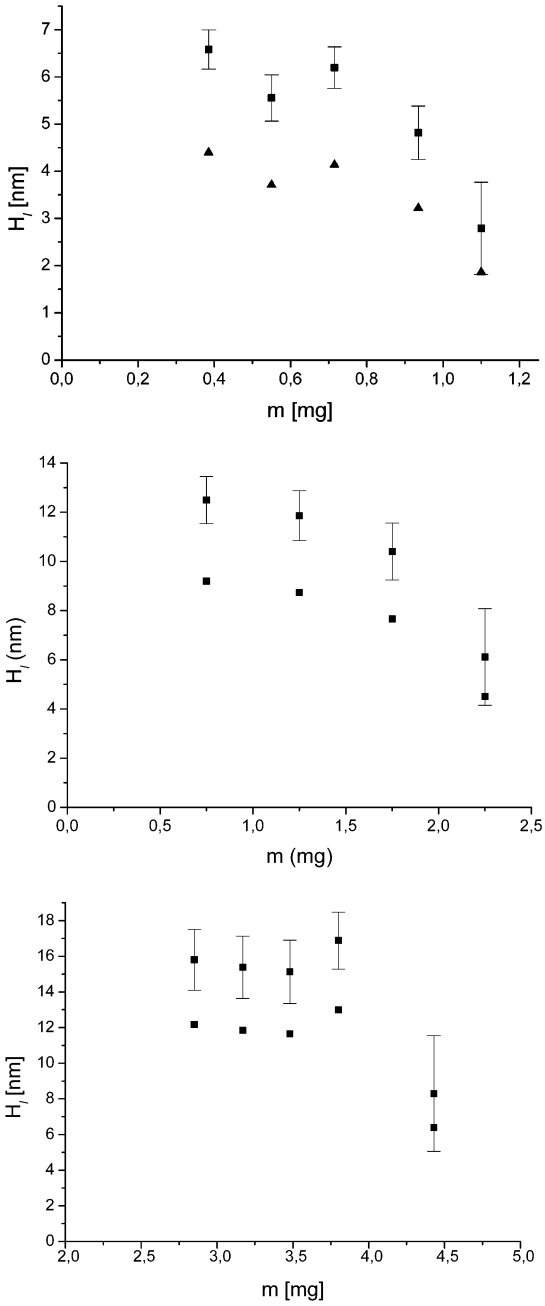

Figure 6. Particle−particle distances (H_l) at the secondary energy minimum of the total pair-potential energy functions at different amounts of spread particles. (■): experimentally determined values; (▲): corrected values. The functions (from top to bottom) belong to the S40, S100 and S200 particles (see text).

gradient of the particles' surface concentration. Hence, the correct value of H_l can be determined, similarly as with the contact angles,[48] by extrapolating to zero amount of particles. The resulting data (H_{l0}) are given in Table 3.

As was mentioned, hydration repulsion cannot be predicted from the experimentally determined water contact angles (61−69°, Table 2). Moreover, the extrapolated values of $H_{l0}/2$ (3.3, 6.5, 8.2 nm for the different sized particles) seem too high to be the bound hydration layer around the particles showing only partial water wettability.[73] Also, the particle size dependence of the thickness of the hydration shell would not be understandable. The hydrodynamic resistance of the water interlayer also cannot be a relevant parameter at the repulsion observed. The velocity of the particles' motion at the present compression rate is lower than if it had originated from the Brownian motion of

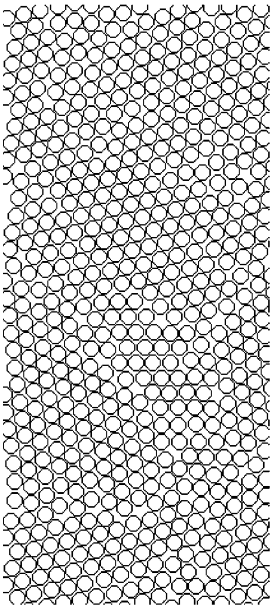

Figure 7. Computer simulated structure of monodisperse spheres near the collapse pressure.

particles considering an averaged kinetic energy of particles, kT. It means the experimentally determined interaction energies cannot be interpreted in terms of the DLVO and hydration repulsion energies even for the smallest particles investigated in the present work (also see the $(F/r)_c$ values in Table 3). It might be attributed to the electrostatic dipole−dipole repulsion. As was emphasized earlier,[71] there can be a secondary energy minimum between the interfacial particles that can be attributed to the dipole−dipole repulsion and capillary attraction. The latter is due to the irregular shape of the three-phase contact lines around the interacting particles. This secondary energy minimum is of non-DLVO origin and the corresponding p−p distance is about a sphere diameter.[72] The significantly smaller p−p distances at the secondary energy minimum found in the present case might be attributed to the diminished dipole−dipole repulsion because of the low ionic strength[64] of the applied subphase.

The Correction of the p−p Distances at the Secondary Minimum of Interparticle Energies: the Results of Computer Simulations. To clarify the effect of model assumptions (perfectly hexagonal array of monodisperse spheres) on the calculated H_l and H_{l0} values, we carried out computer simulations. The experimentally obtained $V_T(H)$ data were fitted by exponential functions that were used in the computer simulations. According to the computer simulations, the compression of randomly situated monodisperse spheres results in a domain structure of particulate film as can be seen in Figure 7. Because of this structure formation in Figure 7, which is in a good agreement with other results,[53] the maximum surface coverage of particles is less than 90.7%, which means we overestimated the p−p distances at the secondary energy minimum. Using the computer simulation, however, we can assess the error of the model assumptions as follows:

As was mentioned, we calculated the p−p interactions from the experimentally obtained $\Pi-A$ isotherms and the potential functions were used in the computer simulation. If the particles were monodisperse and formed a perfectly hexagonal array during the whole compression, we got the experimentally obtained isotherm, A_k and H_l values (for a demonstration see the first step in Figure 8 for S40 particles at the spread amount of 0.4 mg). However, if the particles with real polydispersity

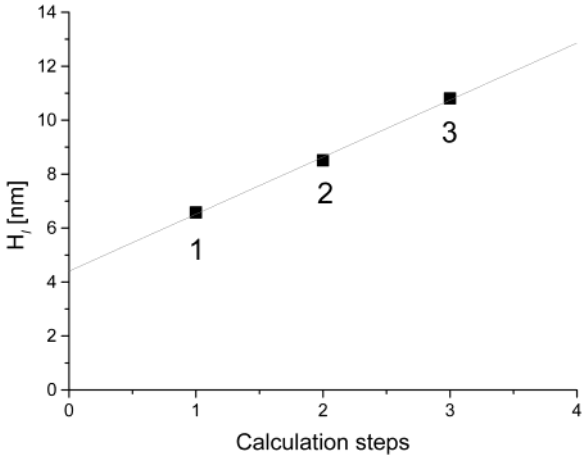

Figure 8. Demonstration for the correction of the H_l value by using computer simulation. (Sample S40; the amount of spread particles: 0.4 mg).

were scattered randomly on the surface, the simulation resulted in a different isotherm with a larger A_k, from which a larger H_l value was obtained (the second step in Figure 8) applying an average particle size and perfectly hexagonal ordering assumptions in the calculation. We determined the p−p interaction from this latter isotherm and made a new simulation with this potential energy using a random scattering of polydisperse particles. We got a new isotherm and a larger H_l value based on ideal assumptions (the third step in Figure 8). Repeating the above simulation steps and plotting the H_l values against the steps, we got a nearly linear function (Figure 8). Extrapolating this function to zero step, a more correct p−p distance could be obtained for a certain amount of spread particles. Making the determinations at different amounts of spread particles, we got a corrected function of H_l values dependence (Figure 6a−c marked with ▲). The extrapolated values of H_{l0corr} are also shown in Table 3. The corresponding lyosphere thickness values (2.2, 4.7, 6.8 nm) still seem too large to be bound hydration layers, especially for the bigger particles, and the particle size dependence would also remain in question.

Conclusion

The interaction of nanoparticles floating at air−water interfaces was studied by using a Wilhelmy film balance and computer simulation. The model particles, different sized Stöber silica nanospheres having diameters of ca. 40, 100, and 200 nm, were seen to form a weakly cohesive layer during the compression; hence, the surface pressure of the film can be considered as a consequence of p−p repulsion.

In this work, we gave further experimental evidence for the existence of recently recognized attractive (1) and repulsive (2) interactions from the pressure−area isotherms of Stöber silica nanoparticles. Moreover, we corrected the experimentally determined values of the p−p distances at the secondary minimum of interparticle energy (3).

(1) According to the BAM investigations, the silica particles, independently of their sizes, formed flocculated−weakly cohesive domains following the spreading. The flocculation could be explained neither by the DLVO nor the hydrophobic attractive forces. It was explained by newly recognized, attractive interparticle forces that were attributed to the irregular shape of the meniscus around the floating particles acting even among nanoparticles or to electrostatic forces because of the periodic arrangement of particles and their counterions.

(2) Analyzing the surface pressure versus surface area isotherms, the interparticle repulsive energies versus p−p distances were determined by an extrapolation method and compared to the results of the calculated DLVO energies. The experimentally determined, extremely high repulsion could not be explained in terms of the DLVO and hydration forces. The repulsion increase during the compression of the monoparticulate films was attributed to dipole−dipole interparticle forces.

(3) We proposed a computer simulation-assisted method to estimate the error of assuming a hexagonal array of monodisperse particles, so that it could be taken into account in the calculation of the p−p distances determined from the pressure−area isotherms.

Acknowledgment. This work was supported by the Hungarian National Scientific Foundation for Research (OTKA T023080 and T030457) and by the Educational Ministry (FKFP 0532/2000).

References and Notes

(1) Binks, B. P. *Curr. Opin. Colloid Interface Sci.* **2002**, *7*, 21.
(2) Allain, C.; Jouhier, B. *J. Phys. (France) Lett.* **1983**, *44*, l.
(3) Hurd, A. J.; Schaefer, D. W. *Phys. Rev. Lett.* **1985**, *54*, 1043.
(4) Skjeltorp, A. T. *Phys. Rev. Lett.* **1987**, *58*, 1444.
(5) Meakin, P. *Adv. Colloid Interface Sci.* **1988**, *28*, 249.
(6) Skjeltorp, A. T.; Helgesen, G. *NATO ASI Ser. E* **1988**, *157*, 56.
(7) Roussel, J.-F.; Camoin, C.; Blanc, R. *J. Phys. (Paris)* **1989**, *50*, 3259.
(8) Roussel, J.-F.; Camoin, C.; Blanc, R. *J. Phys. (Paris)* **1989**, *50*, 3269.
(9) Robinson, D. J.; Earnshaw, J. C. *Phys. Rev. A* **1992**, *46*, 2045.
(10) Robinson, D. J.; Earnshaw, J. C. *Phys. Rev. A* **1992**, *46*, 2055.
(11) Robinson, D. J.; Earnshaw, J. C. *Phys. Rev. A* **1992**, *46*, 2065.
(12) Williams, D. F.; Berg, J. C. *J. Colloid Interface Sci.* **1992**, *152*, 218.
(13) Robinson, D. J.; Earnshaw, J. C. *Langmuir* **1993**, *9*, 1436.
(14) Kralchevsky, P. A.; Nagayama, K. *Langmuir* **1994**, *10*, 23.
(15) Hidalgo-Álvarez, R.; Martin, A.; Fernandez, A.; Bastos, D.; Martinez, F.; de las Nieves, F. J. *Adv. Coll. Interface Sci.* **1996**, *67*, 1.
(16) Hansen, P. H. F.; Bergström, L. J. *Colloid Interface Sci.* **1999**, *218*, 77.
(17) Moncho-Jordá, A.; Odriozola, G.; Martínez-López, F.; Schmitt, A.; Hidalgo-Álvarez, R. *Eur. Phys. J. E* **2001**, *5*, 471.
(18) Onoda, G. Y. *Phys. Rev. Lett.* **1985**, *55*, 2263.
(19) Ghezzi, F.; Earnshaw, J. C. *J. Phys. Condens. Matter* **1997**, *9*, L517.
(20) Tolnai, Gy.; Csempesz, F.; Kabai-Faix, M.; Kálmán, E.; Keresztes, Zs.; Kovács, A. L.; Ramsden, J. J.; Hórvölgyi, Z. *Langmuir* **2001**, *17* (9), 2683.
(21) Wolert, E.; Setz, S. M.; Underhill, R. S.; Duran, R.S *Langmuir* **2001**, *17*, 5671.
(22) Schwartz, H.; Harel, Y.; Efrima, S. *Langmuir* **2001**, *17*, 3884.
(23) Hansen, P. H.; Rödner, S.; Bergström, L. *Langmuir* **2001**, *17*, 4867.
(24) Szekeres, M.; Kamalin, O.; Schoonheydt, R. A.; Wostyn, K.; Clays, K.; Persoons, A.; Dékány, I. *J. Mater. Chem.* **2002**, *12* (11), 3268.
(25) Armstrong, A. J.; Mockler, R. C.; O'Sullivan, W. J. *J. Phys.: Condens. Matter* **1989**, *1*, 1707.
(26) Menon, V. B.; Nikolov, A. D.; Wasan, D. T. *J. Colloid Interface Sci.* **1988**, *124*, 317.
(27) Levine, S.; Bowen, B. D. *Colloids Surf., A* **1993**, *70*, 33.
(28) Aveyard, R.; Clint, J. H. *J. Chem. Soc., Faraday Trans.* **1995**, *91*, 2681.
(29) Aveyard, R.; Beake, B. D.; Clint, J. H. *J. Chem. Soc., Faraday Trans.* **1996**, *92*, 4271.
(30) Meldrum, F. C.; Kotov, N. A.; Fendler, J. H. *J. Phys. Chem.* **1994**, *98*, 4506.
(31) Kotov, N. A.; Meldrum, F. C.; Wu, C.; Fendler, J. H. *J. Phys. Chem.* **1994**, *98*, 2735.
(32) Yi, K.; Hórvölgyi, Z.; Fendler, J. H. *J. Phys. Chem.* **1994**, *98*, 3872.
(33) Fendler, J. H.; Meldrum, F. C. *Adv. Mater.* **1995**, *7*, 607.
(34) Fulda, K.-U.; Tieke, B. *Supramol. Sci.* **1997**, *4*, 265.
(35) Xu, H.; Goedel, W. A. *Langmuir* **2002**, *18* (6), 2363.
(36) Aveyard, R.; Binks, B. P.; Fletcher, P. D. I.; Rutherford, C. E. *Colloids Surf., A* **1994**, *83*, 89.
(37) Hadjiiski, A.; Dimova, R.; Denkov, N. D.; Ivanov, I. B.; Borwankar, R. *Langmuir* **1996**, *12*, 6665.
(38) Hórvölgyi, Z.; Németh, S.; Fendler, J. H. *Langmuir* **1996**, *12*, 997.
(39) Wills, B. A. In *Mineral Processing Technology*; Hopkins, D. W., Ed.; Int. Ser. Materials Science and Technology, Vol. 41; Pergamon Press: Oxford, 1988; p 457.
(40) Fuerstenau, D. W.; Herrera-Urbina, R. In *Mineral Separation by Froth Flotation: Surfactant-Based Separation Processes*; Scamehorn, J. F., Harwell, J. F., Eds.; Surfactant Sci. Ser., Vol. 33; Marcel Dekker: New York and Basel, 1989; p 259.
(41) Schuller, H.; Kolloid, Z. Z. *Polymer* **1967**, *380*, 216−217, 380.
(42) Sheppard, E.; Tcheurekdjian, N. *J. Colloid Interface Sci.* **1968**, *28*, 481.
(43) Doroszkowski, A.; Lambourne, R. *J. Polym. Sci., Part C* **1971**, *34*, 253.
(44) Garvey, M. J.; Mitchell, D.; Smith, A. L. *Colloid Polym. Sci.* **1979**, *257*, 70.
(45) Clint, J. H.; Taylor, S. E. *Colloids Surf.* **1992**, *65*, 61.
(46) Olugebefola, S. C.; Park, S. Y.; Banerjee, P.; Mayes, A. M. *Langmuir* **2002**, *18*, 1098.
(47) Derjaguin, B. V.; Churaev, N. V. *Colloids Surf.* **1989**, *41*, 223.
(48) Máté, M.; Fendler, J. H.; Ramsden, J. J.; Szalma, J.; Hórvölgyi, Z. *Langmuir* **1998**, *14*, 6501.
(49) Máté, M.; Zrínyi, M.; Hórvölgyi, Z. *Colloids Surf., A* **1996**, *108*, 147.
(50) Seebergh, J. E.; Berg, J. C. *Colloids Surf., A* **1995**, *100*, 139.
(51) Aveyard, R.; Clint, J. H.; Nees, D.; Paunov, V. N. *Langmuir* **2000**, *16*, 1969.
(52) Aveyard, R.; Clint, J. H.; Nees, D.; Quirke, N. *Langmuir* **2000**, *16*, 8820.
(53) Sun, J.; Stirner, T. *Langmuir* **2001**, *17*, 3103.
(54) Fenwick, N. I. D.; Bresme, F.; Quirke, N. *J. Chem. Phys.* **2001**, *114* (16), 7274.
(55) Pieranski, P. *Phys. Rev. Lett.* **1980**, *45*, 569.
(56) Quesada-Pérez, M.; Moncho-Jordá, A.; Martínez-López, F.; Hidalgo-Álvarez, R. *J. Chem. Phys.* **2001**, *115* (23), 10897.
(57) Stöber, W.; Fink, A.; Bohn, E. *J. Colloid Interface Sci.* **1968**, *26*, 62.
(58) Bailey, J. K.; Mecartney, M. L. *Colloids Surf.* **1992**, *63*, 151.
(59) Kabai-Faix, M. *Magy. Kem. Foly.* **1996**, *102* (1), 33.
(60) Clint, J. H.; Quirke, N. *J. Colloids Surf. A: Physicochem. Eng. Asp.* **1993**, *78*, 277.
(61) Meunier, J.; Henon, S. *Prog. Colloid Polym. Sci.* **1991**, *84*, 194.
(62) Cacace, M. G.; Landau, E. M.; Ramsden, J. J. *Q. Rev. Biophys.* **1997**, *30*, 241.
(63) Martínez-López, F.; Cabrerizo-Vílchez, M. A.; Hidalgo-Álvarez, R. *J. Colloid Interface Sci.* **2000**, *232*, 303.
(64) Moncho-Jordá, A.; Martínez-López, F.; González, A. E.; Hidalgo-Álvarez, R. *Langmuir* **2002**, *18*, 9183.
(65) Chan, D. Y. C.; Henry, J. D., Jr.; White, L. R. *J. Colloid Interface Sci.* **1981**, *79*, 410.
(66) Ludwig, P.; Peschel, G. *Prog. Colloid Polym. Sci.* **1988**, *77*, 146.
(67) Verwey, E. J. W.; Overbeek, J. Th. G. *Theory of the stability of lyophobic colloids*; Elsevier Publishing Company: Amsterdam−New York, 1948; p 152.
(68) Csempesz, F.; Hórvölgyi, Z. unpublished.
(69) Rapaport, D. C. *The Art of Molecular Dynamics Simulation*; Cambridge University Press: 2001.
(70) Hórvölgyi, Z.; Medveczky, G.; Zrínyi, M. *Colloid Polym. Sci.* **1993**, *271*, 396.
(71) Levine, S.; Bowen, B. D.; Partridge, S. *J. Colloid Surf.* **1989**, *38*, 325.
(72) Stamou, D.; Duschl, C.; Johannsmann, D. *Phys. Rev. E* **2000**, *62* (4), 5263.
(73) Israelachvili, J. N. *Intermolecular and Surface Forces*, 2nd edition; Academic Press: London, San Diego, New York, Boston, Sydney, Tokyo, Toronto, 1991; p. 277.
(74) Hórvölgyi, Z.; Németh, S.; Fendler, J. H. *Colloids Surf. A: Physicochem. Eng. Asp.* **1993**, *71*, 327.